ELSEVIER

Fluid Dynamics Research 28 (2001) 267–280

FLUID DYNAMICS RESEARCH

Experimental and theoretical study of the flow in the volute of a low specific-speed pump

J.D.H. Kelder [1], R.J.H. Dijkers [2], B.P.M. van Esch [3], N.P. Kruyt *

Department of Mechanical Engineering, University of Twente, P.O. Box 217, 7500 AE Enschede, Netherlands

Received 5 November 1999; received in revised form 8 May 2000; accepted 25 August 2000

Abstract

The flow in the volute of a low specific-speed pump was studied both experimentally and numerically near its design point. Measurements included time-averaged values of velocity and static pressure at a large number of locations in the volute. The numerical computations were based on the unsteady three-dimensional potential flow model for the core flow. Viscous losses were quantified using additional models that use the potential flow as input. It is shown that near the design point of this pump, the core flow behaves like a potential flow, provided that no boundary layer separation occurs. Explanations are given for the presence of local deviations due to secondary flow. These local deviations do not influence the overall potential flow characteristics significantly. © 2001 Published by The Japan Society of Fluid Mechanics and Elsevier Science B.V. All rights reserved.

Keywords: Centrifugal pump; Volute; Velocity measurement; Potential flow

1. Introduction

In order to improve the design of centrifugal pumps and compressors, a better understanding of the flow of such machines is required. This paper deals with an experimental and theoretical study of the flow in the volute of a low specific-speed centrifugal pump. Extensive measurements have been performed of both velocities and pressures. The unsteady flow in the impeller–volute combination is also computed, using the potential flow model. Additional models are used to quantify viscous losses.

For pumps operating *near their design point* the influence of viscosity is restricted to thin boundary layers and wakes, provided no massive boundary layer separation occurs. The core of the flow

* Corresponding author. Tel.: +31-53-489-2528; fax: +31-53-489-3695.
E-mail address: n.p.kruyt@wb.utwente.nl (N.P. Kruyt).
[1] Current address. Faculteit Scheikundige Technologie, Technische Universiteit Eindhoven, P.O. Box 513, 5600 MB Eindhoven, Netherlands.
[2] Current address. Flowserve Corporation, P.O. Box 55, 7550 AB Hengelo, Netherlands.
[3] Current address. Faculteit Werktuigbouwkunde, Technische Universiteit Eindhoven, P.O. Box 513, 5600 MB Eindhoven, Netherlands.

0169-5983/01/$20.00 © 2001 Published by The Japan Society of Fluid Mechanics and Elsevier Science B.V. All rights reserved.
PII: S0169-5983(00)00032-0

can then be predicted fairly accurately by means of three-dimensional inviscid methods. If one further assumes the incoming flow to be irrotational, the core of the flow can be modelled as an incompressible potential flow.

Contrary to methods based on the potential flow model, current methods based on the Navier–Stokes equations with turbulence models (for example, Dawes, 1995; Croba and Kueny, 1996) are of limited suitability as part of a *design tool* given their extreme requirements in terms of computer resources. In addition, other open problems in such computations are (see Guelich, 1999): (i) accurate modelling of boundary layer transition and separation (Casey et al., 1995); (ii) the choice of an appropriate turbulence model that accounts for the effects of three-dimensional boundary layers, curvature and rotation (Speziale, 1985; Rodi, 1986; Speziale, 1989; Lakshminarayana, 1991; Schilling, 1994); (iii) interaction between impeller and diffusor (Guelich and Egger, 1992); and (iv) influence of mesh size near solid walls on predictions (Guelich et al., 1997). Therefore the potential flow model with viscous corrections is suitable for conditions *near the design point*, while the turbulent viscous models are suitable for a somewhat wider range of flow conditions, although at a much higher cost. Examples of the capabilities of the potential flow model with viscous corrections as a *design tool* for complex three-dimensional impellers are given by Dijkers et al. (2000).

Previous studies on the flow in volutes dealing with the effect of volute geometry on overall characteristics (head and efficiency versus capacity curves) were performed by Bowerman and Acosta (1957), Rütschi (1961), Worster (1963) and Decker (1990).

Measurements of velocities in a volute were presented by Sideris and van den Braembussche (1987), Paone et al. (1989), Miner et al. (1989) and Flack et al. (1992). The pressure distribution around the impeller is of importance for the radial forces acting on the impeller (Iversen et al., 1960; Lorett and Gopalakrishnan, 1986; Sideris and van den Braembussche, 1987; Ojeda et al., 1992).

Design methods for volutes are usually based either on the assumption of constant average velocity (Stepanoff, 1948) or on the assumption of constant angular momentum (Pfleiderer, 1949).

From these design methods and from experiments it follows (for example Worster, 1963) that at a single flow rate the pressure along the periphery of the impeller is approximately constant. For lower flow rates the pressure increases from volute inlet (tongue) to volute outlet: the volute acts like a diffuser. For higher flow rates the pressure decreases from volute inlet to volute outlet: the volute acts like a converging nozzle.

The outline of this paper is as follows. Firstly, the test set-up is described, followed by an outline of the computational method. Then the models are described that are used to account for losses due to viscous effects. Finally, the results of both measurements and computations are given and discussed.

2. Test set-up

A detailed description of the test-rig that was built to study the two-dimensional flow in various types of centrifugal impellers is given by Visser et al. (1999). In order to study the interaction between the impeller and the volute of a pump, this test-rig has been adapted to include a volute. In the study by Visser et al. (1999) of the flow in an impeller channel, the laser Doppler velocimetry (LDV) measurement system rotated with the impeller, while in the current study of the flow in the volute, the LDV system is stationary (non-rotating).

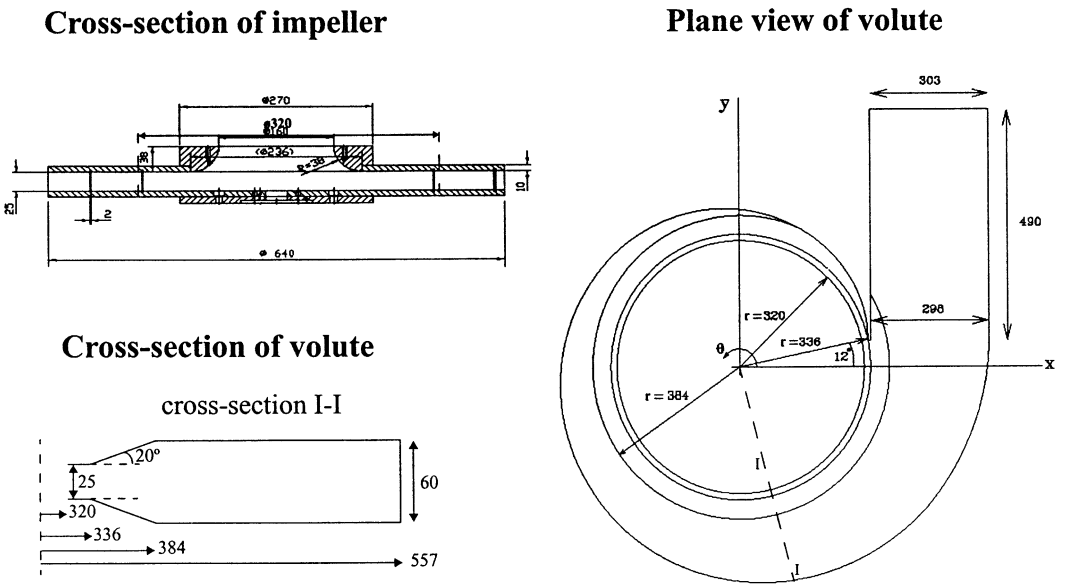

Fig. 1. Geometry of centrifugal impeller (cross-section) and volute (plane view and cross-section). All dimensions in mm.

Measurements were performed with a centrifugal pump (see Fig. 1) having a low specific-speed $n_\omega = (\Omega Q^{1/2})/(gH)^{3/4}$ of 0.4. The impeller has seven blades with a constant blade angle of 70° with respect to the radial direction and a constant blade thickness of 2 mm. The impeller blade inner diameter is 320 mm, its outer diameter 640 mm, and the axial width is 25 mm. The volute has a trapezoidal cross-section and is designed to approximately match the impeller at design condition (design flow rate $Q_d = 0.008$ m^3/s, angular velocity $\Omega = 4.2$ rad/s), according to the method of constant angular momentum (Pfleiderer, 1949). The Reynolds number $(\Omega D^2)/\nu$ is 1.7×10^6, where ν is the kinematic viscosity of water. The volute tongue has a cylindrical shape with a diameter of 2 mm. During construction special attention was paid to the minimization of leakage flows. The pump was operated at flow rates of 82.5 %, 100 % and 117.5% of the design flow rate.

Velocity measurements were performed using LDV. The LDV configuration is described in detail by Visser et al. (1999). It employs a dual reference beam forward scattering system, capable of parallel detection of two perpendicular velocity components. Two Bragg cells were used to effectuate preshifts between main beam and the two reference beams, thus enabling the determination of the direction of the velocity components. Two detectors measured the Doppler frequency. These signals were sampled and stored on disc. Time-averages and RMS-values could be computed. Information on the axial velocity component could not be obtained. U-tube manometers were used to obtain values of the static pressure. Fig. 2 shows the locations in the volute where velocity and static pressure measurements were obtained. At the locations just outside the impeller, the pressure was measured at the shroud side, while at the volute outer wall it was measured at midheight.

The head-capacity curve was derived from the static pressure difference between inlet and outlet of the pump and the assumption of uniform velocity in these regions. It is not possible to measure the hydraulic efficiency of the pump with the current experimental set-up. Air-bubble visualisation was used to investigate the flow near the tongue of the volute.

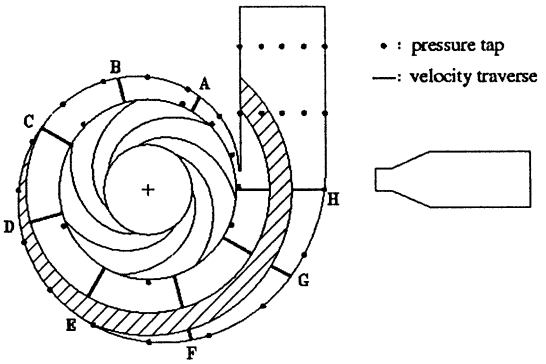

Fig. 2. Measurement locations in the laboratory centrifugal pump. LDV measurements are performed along traverses A to H at the volute centre line. Static pressure measurement locations are indicated with solid markers. The hatched area shows the region which is visually inaccessible.

3. Computational method

In general centrifugal pumps will show unsteady flow behaviour, especially at off-design conditions, as a result of the interaction between impeller and volute. A proper time-dependent matching of the respective computational domains is therefore necessary, which is one of the main objectives of the current method.

3.1. Potential flow model

The Reynolds and Mach numbers for the flow in hydraulic turbomachines are usually such that the core flow can be considered as inviscid and incompressible. Assuming the suction flow to be irrotational, the problem can be formulated in terms of the velocity potential ϕ. The velocity vector $\boldsymbol{v}$ can then be written as

$$\boldsymbol{v} = \nabla\phi \tag{1}$$

and the continuity equation reduces to the Laplace equation

$$\nabla^2\phi = 0. \tag{2}$$

The pressure can be computed from the unsteady Bernoulli equation

$$\frac{\partial\phi}{\partial t} + \frac{1}{2}\,\boldsymbol{v}\cdot\boldsymbol{v} + \frac{p}{\rho} + gz = c(t), \tag{3}$$

where t denotes the time, p the static pressure, ρ the density, g the gravitational acceleration, z the height and c a constant which only depends on time t.

3.2. Computational domain and boundary conditions

In the multi-block approach adopted here, the flow region of interest is divided into subdomains, all having a topologically cubic shape. The subdomains are non-overlapping, with nodal coincidence at the interfaces.

Blocks in the impeller and the volute are separated by a cylindrical or conical surface. At the interface, the values of the potential ϕ at corresponding nodal points from impeller and volute are matched. Note that this correspondence of nodal points is time-dependent. In this way the rotating motion of the impeller relative to the volute is properly simulated without having to create a new mesh for each timestep, as was done by Miner et al. (1992).

Appropriate uniform Neumann boundary conditions are applied at the inlet, outlet and blade surfaces. At block boundaries formed by the wake surfaces emanating from trailing edges, vortices are shed downstream. These vortex sheets are a result of both non-uniform blade loading (variations of the circulation along the blade's span) and time-dependent variations of the blade circulations. Vortex sheets are modelled by imposing discontinuities of the potential value across the wake surface

$$\phi^{+}(r,s,t) = \phi^{-}(r,s,t) + \gamma(r,s,t), \tag{4}$$

where the two sides of the wake are denoted by the '+' and '−', and r and s are local coordinates in the wake. By allowing the potential jump γ to vary along the vortex sheet, a discontinuity of the tangential velocity across the wake is introduced. The value of the potential jump and its variation is computed by determining the amount of circulation around the blade(s) that is needed to satisfy Kutta's condition of smooth flow from the trailing edges. In steady computations, the potential jumps will be constant along streamlines, whereas in unsteady computations the time-dependent variation of the blade circulation is convected downstream with the mean velocity relative to the rotating impeller.

3.3. Numerical method

The numerical method is based on a fully three-dimensional finite element method. Some special techniques are employed in order to reduce computing time and memory requirements. These are based on a superelement approach (Zienkiewicz and Taylor, 1989) in conjunction with implicitly solved values of blade circulations. A fully three-dimensional method was used to account for the three-dimensional parts of the geometry: the inlet and the volute region where the volute width varies (see Fig. 1).

The superelement approach greatly facilitates the time-dependent coupling of the rotating impeller to the stationary volute, which is essential in a correct description of the interaction between impeller and volute. In the superelement approach internal degrees of freedom (DOFs) are expressed in terms of DOFs that are located at the boundary of the superelements. The time-invariant nature of this elimination process implies that unsteady computations can be performed with far fewer DOFs. Furthermore, this elimination process is identical for geometrically similar superelements, such as the impeller channels.

By considering the unknown circulations around the blades as additional DOFs in the finite element solution process, the Kutta conditions can be imposed implicitly. This avoids the need to compute a large number of subpotentials, which is especially important in three-dimensional computations since the number of unknown circulation values is much larger.

A detailed description of the numerical method is given in Kruyt et al. (1999). Here its main advantages are summarized:

- Impeller symmetry is fully exploited.
- Superelement matrices have to be computed only once for unsteady computations.

- Kutta conditions at the trailing edges are imposed implicitly.
- The number of DOFs is greatly reduced in unsteady computations.

4. Viscous loss models

Inviscid methods will always over-predict a pump's head, while being unable to predict its efficiency. The obvious reason is that viscous losses are not taken into account. A very efficient way to incorporate the effects of viscosity is to use an inviscid method along with additional models to estimate the viscous losses. Many of these (well-established) models exist in the literature (see, for example, Denton, 1993), for which most of the input can be supplied by potential flow analysis. The models are adopted here without adjusting the empirical coefficients.

Pump power losses are commonly classified as:

- Hydraulic losses.
- Volumetric losses.
- Disc friction losses.
- Mechanical losses.

In the absence of leakage flows, the head is numerically determined by

$$H = \frac{\Omega M - P_{\mathrm{L,h}}}{\rho g Q}, \tag{5}$$

where Ω is the angular velocity, Q is the flow rate, $P_{\mathrm{L,h}}$ is the hydraulic power loss, and M is the moment exerted by the impeller blades on the fluid. The latter can be computed by an inviscid numerical method. External losses due to disc friction and mechanical losses need not be considered here. All quantities are time-averaged. Existing models to quantify the above-mentioned losses will now be presented.

Hydraulic power losses for this configuration are composed of dissipative losses in the boundary layers $P_{\mathrm{L,diss}}$ along walls in both the impeller and the pump casing, and mixing losses $P_{\mathrm{L,mix}}$ in wakes

$$P_{\mathrm{L,h}} = P_{\mathrm{L,diss}} + P_{\mathrm{L,mix}}. \tag{6}$$

The dissipation power loss in attached boundary layers can be quantified using a fairly simple method based on dissipation coefficients (Schlichting, 1979). The dissipation loss is written as

$$P_{\mathrm{L,diss}} = \tfrac{1}{2}\rho \int_S c_{\mathrm{D}} w^3 \,\mathrm{d}S, \tag{7}$$

where S denotes the wall surface, c_{D} is the dissipation coefficient and w is the velocity of an inviscid flow tangential to the wall. According to Denton (1993) the dissipation coefficient for turbulent boundary layers is relatively insensitive to the detailed state of the boundary layer (accelerating or decelerating). Denton suggests an average value of 0.0038 for turbulent boundary layers with Re_θ (Reynolds number based on boundary layer momentum thickness) of order 1000, but it should be stressed that actual values vary between 0.002 for accelerating flows and 0.005 for flows encountering an adverse pressure gradient. As a first estimate boundary layers, both in the impeller and in the volute, are assumed to be turbulent, with $c_{\mathrm{D}} = 0.0038$.

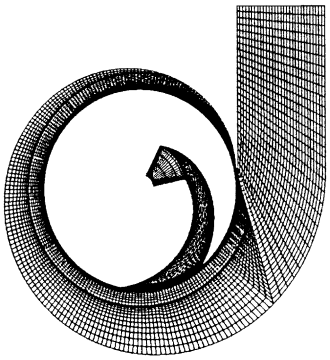

Fig. 3. Plane view of the computational mesh for the centrifugal pump with spiral volute. Only one of the seven impeller channels is shown.

Mixing losses occur in wakes behind blunt trailing edges of impeller (or stator) blades. According to Denton (1993) the loss can be quantified using

$$P_{\mathrm{L,mix}} = \frac{1}{2}\rho w_{\mathrm{ref}}^2 Q\left[-\frac{C_{\mathrm{pb}}b}{W} + \frac{2\theta}{W} + \left(\frac{\delta^* + b}{W}\right)^2\right], \tag{8}$$

with b the blade thickness and W the blade pitch. The sum of the momentum thicknesses at pressure and suction side, at a station near the trailing edge, is given by θ. The same applies to δ^*, the sum of the displacement thicknesses. The base pressure coefficient C_{pb} is defined by

$$C_{\mathrm{pb}} = \frac{p_{\mathrm{b}} - p_{\mathrm{ref}}}{1/2\rho w_{\mathrm{ref}}^2}, \tag{9}$$

with p_{b} the static pressure just behind the trailing edge and p_{ref} and w_{ref} the pressure and velocity at a reference position just before the trailing edge. In general, the value of C_{pb} will be negative, with typical values close to -0.15.

The boundary layer displacement and momentum thickness at the blade trailing edge are computed by a one-dimensional integral boundary layer method. The method of Thwaites (1949) is used for the laminar part of the boundary layer, while Green's "lag entrainment method" (Green et al., 1972) is used for the turbulent part. Michel's criterion (Michel, 1952) is used to determine the location of transition. Thwaites' criterion is implemented to predict laminar separation. The boundary layer changes to a turbulent state either after laminar separation or transition. Turbulent separation is assumed to occur when the shape factor (ratio of displacement thickness and momentum thickness) exceeds the value of 2.8.

Of both hydraulic losses mentioned in this section, boundary layer dissipation is the most important loss mechanism.

5. Results

In this section the results of measurements and computations are compared. These results deal with velocities, pressures and overall characteristics. The computational mesh is shown in Fig. 3.

It contains a total of 168,000 nodes, of which 14,500 are located in each of the seven impeller channels. Computations are performed with 105 timesteps per shaft revolution.

5.1. Velocity in the volute

Radial and circumferential velocity components were measured in a plane at the centre of the volute. The traverses *A–H* (see Fig. 2) were scanned for the low flow rate $Q = 0.825Q_d$, the design flow rate Q_d and the high flow rate $Q = 1.1175Q_d$.

Typical results are shown in Fig. 4, together with the time-averaged computed values. The full set of measurements and computations is presented in Kelder (1996). In a large region of the volute (60–285° from the tongue) computed circumferential velocities agree very well with measurements at design flow conditions. For the low flow rate this excellent agreement is restricted to a smaller region (150–285° from the tongue). For high flow rate the agreement is not very good except for a small region 60–150° from the tongue. The agreement between computed and measured radial velocities is poor.

This discrepancy was further investigated by performing traverses over the width of the volute. Results are given in Fig. 5 which shows the variation of normalised radial and circumferential velocity over the width of the volute for two radial positions on cross-section *F* (see Fig. 2). The circumferential velocity is practically constant over the width of the volute, while the (much smaller) radial velocity shows severe secondary flow. Note that the circumferential velocity determines the energy transfer by the impeller blades to the fluid. The computed radial and circumferential velocities were practically constant over the width of the volute.

5.2. Static pressure in the volute

The static pressure difference Δp between the inlet of the pump and locations in the volute is measured using U-tube manometers. It is made non-dimensional with the blade-tip speed according to

$$\Delta p = \frac{p_{vol} - p_{inlet}}{\rho(\Omega r_{TE})^2}. \tag{10}$$

In Fig. 6 results of measurements and computations are shown for locations just outside the impeller and along the volute outer wall, for three different flow rates. The inviscid computations lead to pressure values which, on average, are too high. However, in a large region, not too near to the tongue, the qualitative agreement is quite good. A constant static pressure around the impeller can be observed at design flow rate.

The computed static pressure values can be corrected for viscous losses in the impeller

$$\Delta p_{corr} = \Delta p_{invisc} - \rho g \Delta H_{L,h,imp}, \tag{11}$$

where the hydraulic head loss in the impeller is denoted by $\Delta H_{L,h,imp}$. By doing so, the agreement is improved, although deviations still occur at off-design conditions.

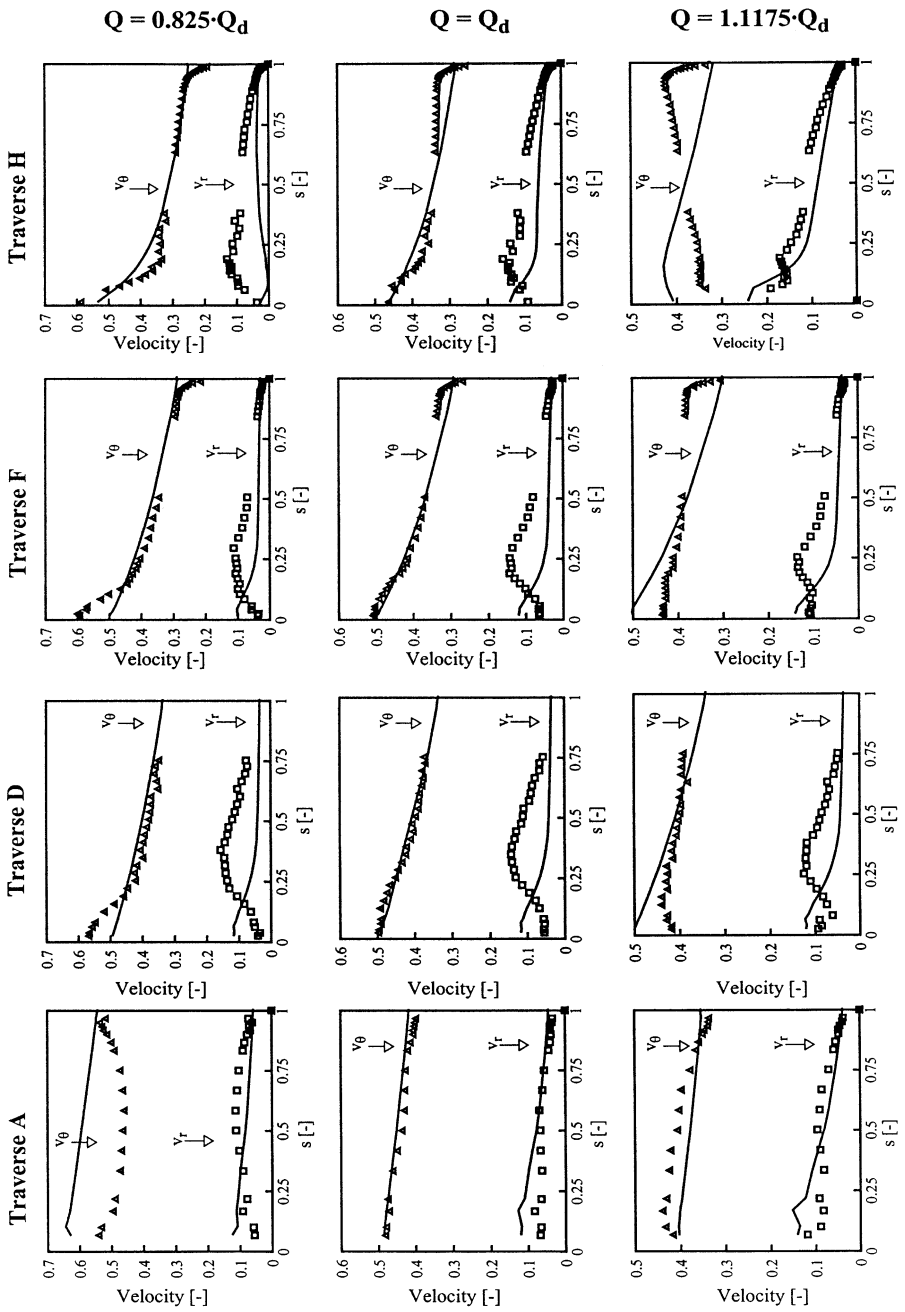

Fig. 4. Non-dimensional radial and circumferential velocity in the volute along different traverses for three flow rates. Comparison between measurements (symbols) and computations (solid line). The scaled local coordinate along the traverse is denoted by s, ranging from 0 at the impeller outer radius to 1 at the volute wall. Velocities are scaled with blade tip speed.

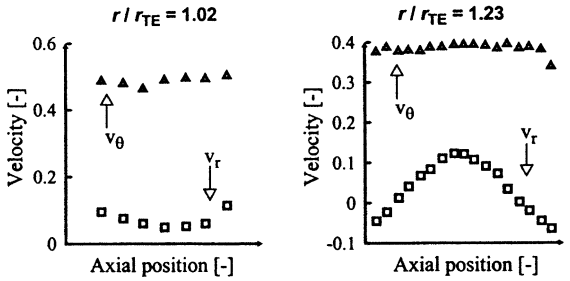

Fig. 5. Variation of radial and circumferential velocities with axial position for two radial positions on traverse F (blade tip radius denoted by r_{TE}). Velocities are scaled with blade tip speed.

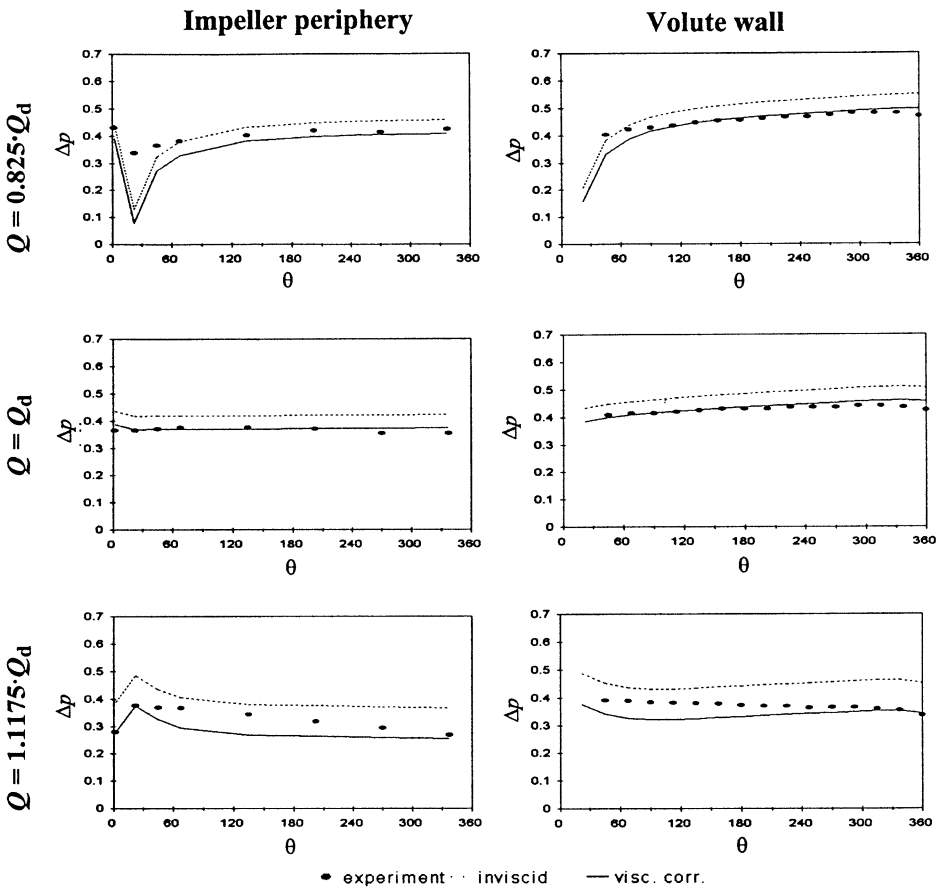

Fig. 6. Static pressure difference in the volute of the laboratory centrifugal pump as a function of orientation θ (degrees), for three flow rates. See Fig. 2 for locations at the impeller periphery and the volute wall. Pressure difference Δp is defined in Eqs. (10) and (11).

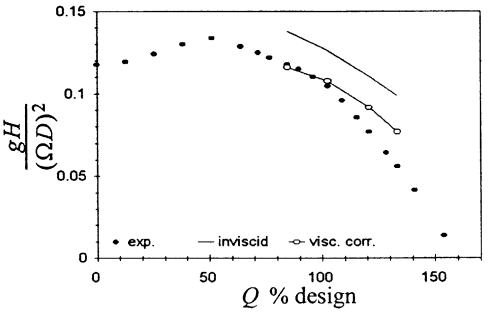

Fig. 7. Head-capacity curve for the centrifugal pump, showing measured and computed values, both inviscid and corrected for viscous losses.

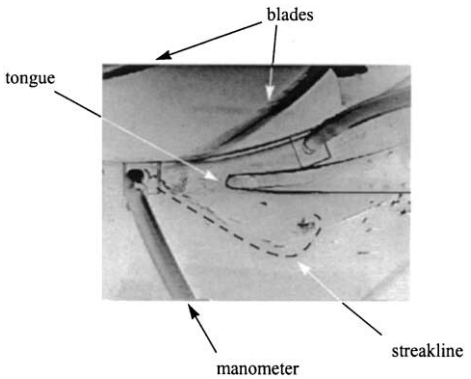

Fig. 8. Photograph of the flow near the tongue of the volute at $Q = 1.1175Q_d$ showing boundary layer separation. Air bubbles were inserted through the manometer for flow visualisation.

5.3. Head curve

The methods described in Section 4 are used to quantify the effects of boundary layer dissipation and wake mixing. The resulting head-capacity curve is shown in Fig. 7. The fraction of the total head loss caused by wake mixing ranges from 10% at high mass flow to 25% at low mass flow.

5.4. Air bubble visualisation

The flow around the volute tongue was visualised using air bubbles that were injected into the flow (see also Fig. 8).

For the low flow rate $Q = 0.825Q_d$, the pressure around the impeller increases from tongue towards the outlet (see Fig. 6). The stagnation point near the tongue will be located towards the throat. Bubbles injected into the flow will therefore pass the tongue on the impeller side, consistent with the visualisations.

For the design flow rate Q_d, the stagnation point is (on average) located on the volute tongue, and due to the time-dependent nature of the flow, half of the bubbles pass the tongue on the impeller side and half pass on the outlet side.

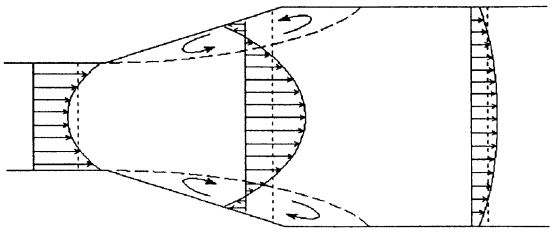

Fig. 9. Cross-section of the volute, showing measured radial velocity profiles. Average velocities are indicated by dotted lines.

For the high flow rate $Q = 1.1175Q_d$, a recirculation zone is observed in the volute throat downstream of the volute tongue, indicating boundary layer separation. This phenomenon of boundary layer separation near the tongue for large flow rates was also noted by Wo and Bons (1993).

6. Discussion

In this section explanations are sought for the differences between measurements and computations. An investigation of the axial distribution of radial velocities at a number of radial positions in the impeller and the volute reveals that a region of severe secondary flow is located in the volute. Typical radial velocity profiles are sketched in Fig. 9. The observed convex radial velocity profile in the volute region, with negative velocities near the upper and lower surfaces, can be explained by an analysis of pressure forces and centrifugal forces (due to curvature) in the boundary layers and the main flow. It is equivalent to the secondary flow encountered in the flow through a pipe bend. A similar analysis for the flow through the impeller can be made (see, for example, Lakshminarayana, 1996), where the additional centrifugal force due to rotation and the Coriolis force have to be taken into account. The equilibrium between pressure forces and Coriolis forces in the main flow is lost in the boundary layers at hub and shroud surfaces, leading to a secondary flow in the boundary layers directed from pressure to suction side. In the main flow a reverse secondary flow direction is observed. This leads to the observed concave radial velocity profile for impellers with backward curved blades.

The secondary flow does not seem to influence the static pressure distribution. Except for the high flow rate, the agreement between measurements and potential flow computations (after correcting for viscous losses in the impeller) is quite good. It can be seen from the difference between both that viscous losses build up as the fluid is flowing along the volute wall from the tongue to the volute throat.

Similar results are obtained for the head-capacity curve. The good agreement at low and design flow rate imply that other sources of viscous losses are not very important in this pump. At high-flow rate, however, a larger deviation is observed between computations and experiments.

A possible cause for the disagreement between measurements and computations at the high-flow rate is boundary layer separation at the exhaust pipe, downstream of the tongue, that was observed by the air-bubble flow visualisation.

The blockage effect resulting from the separated boundary layer could well be related to the observed circumferential velocity profiles at high flow rate, which deviate considerably from the

computations. A homogeneous distribution of tangential velocity was seen to cover the major part of the volute extending from traverses B to G (Fig. 2). It is suggested by the authors that measured velocity profiles like these have inspired Stepanoff (1957) to put forward his method of constant mean velocity for constructing volutes. A similar flow field can emerge at design flow rate if the volute is designed somewhat too small. It is known that volutes designed according to the method of Stepanoff are smaller than those designed according to the method of constant angular momentum (Pfleiderer, 1949).

References

Bowerman, R.D., Acosta, A.C., 1957. Effect of the volute on performance of a centrifugal pump impeller. Trans. ASME 79, 1057–1069.

Casey, M.V., Eisele, K., Muggli, F.A., Guelich, J., Schachenmann, A., 1995. Flow analysis in a pump diffuser. Part 2: validation of a CFD code for steady flow. ASME FED 227, pp. 135–143.

Croba, D., Kueny, J.L., 1996. Numerical calculation of two-dimensional, unsteady flow in centrifugal pumps: impeller and volute interaction. Int. J. Numer. Methods Fluids 22, 467–482.

Dawes, W.N., 1995. A simulation of the unsteady interaction of a centrifugal impeller with its vaned diffuser: flow analysis. J. Turbomach. 117, 213–222.

Decker, H., 1990. Investigation of the performance of model pumps with semi-open impellers. Ph.D. Thesis, University of Karlsruhe, Germany (in German).

Denton, J.D., 1993. Loss mechanisms in turbomachines. J. Turbomach. 115, 621–656.

Dijkers, R.J.H., Visser, F.C., op de Woerd, J.G.H., 2000. Redesign of a high-energy centrifugal pump first-stage impeller. IAHR Conference 2000, Charlotte, NC, USA, Paper PD-01.

Flack, R.D., Miner, S.M., Beaudoin, R.J., 1992. Turbulence measurements in a centrifugal pump with a synchronously orbiting impeller. J. Turbomach. 114, 350–359.

Green, J.E., Weeks, D.J., Brooman, J.W.F., 1972. Prediction of turbulent boundary layers and wakes in compressible flow by a lag-entrainment method. RAE Technical Report 72231.

Guelich, J.F., 1999. Centrifugal Pumps — A Handbook for Development, Design and Operation. Springer, Berlin, Germany (in German).

Guelich, J.F., Egger, R., 1992. Part load flow and hydraulic stability of centrifugal pumps. EPRI Report TR-100219.

Guelich, J.F., Favre, J.N., Denus, K., 1997. An assessment of pump impeller performance predictions by 3D-Navier–Stokes calculations. ASME FED-SM97, p. 3341.

Iversen, H., Rolling, R.E., Carlson, J.J., 1960. Volute pressure distribution, radial force on the impeller and volute mixing losses of a radial flow impeller. J. Eng. Power 82, 136–144.

Kelder, J.D.H., 1996. Measurements and computations of the flow in a quasi two-dimensional model pump. M.Sc. Thesis, Department of Mechanical Engineering, University of Twente, The Netherlands (in Dutch).

Kruyt, N.P., Esch, B.P.M., van Jonker, J.B., 1999. A superelement-based method for computing unsteady three-dimensional potential flows in hydraulic turbomachines. Comm. Numer. Methods Eng. 15, 381–397.

Lakshminarayana, B., 1991. An assessment of computational fluid dynamic techniques in the analysis of turbomachinery. J. Fluids Eng. 113, 315–352.

Lakshminarayana, B., 1996. Fluid Dynamics and Heat Transfer of Turbomachinery. Wiley, New York.

Lorett, J.A., Gopalakrishnan, S., 1986. Interaction between impeller and volute of pumps at off-design conditions. J. Fluid Eng. 108, 12–18.

Michel, R., 1952. Study of transition on wing sections; establishment of a criterion for the determination of point of transition and calculation of the wake of an incompressible profile. ONERA Report 1/1578A (in French).

Miner, S.M., Beaudoin, R.J., Flack, R.D., 1989. Laser velocimeter measurements in a centrifugal flow pump. J. Turbomach. 111, 205–212.

Miner, S.M., Flack, R.D., Allaire, P.E., 1992. Two-dimensional flow analysis of a laboratory centrifugal pump. J. Turbomach. 114, 333–339.

Ojeda, W., de Flack, R.D., Miner, S.M., 1992. Pressure distributions in a single and two versions of a double volute of a centrifugal pump. Proceedings of International Gas Turbine and Aeroengine Congress and Exposition, 92-GT-20.

Paone, N., Riethmuller, M.L., Braembussche, R.A. van den, 1989. Experimental investigation of the flow in the vaneless diffuser of a centrifugal pump by particle image displacement velocimetry. Exp. Fluids 7, 371–378.

Pfleiderer, C., 1949. Centrifugal Pumps for Liquids and Gases. Springer, Berlin, Germany (in German).

Rodi, W., 1986. Turbulence modelling for incompressible flows. Phys. Chem. Hydrodyn. 7, 297–324.

Rütschi, K., 1961. Influence of volutes on the performance of centrifugal pumps. Schweizerische Bauzeitung 79, 233–240 (in German).

Schlichting, H., 1979. Boundary Layer Theory. McGraw-Hill, New York.

Schilling, R., 1994. A critical review of numerical models predicting the flow through hydraulic machinery bladings. Proceedings of the 17th IAHR Symposium, Beijing, GL2.

Sideris, M.T., van den Braembussche, R.A., 1987. Influence of a circumferential exit pressure distortion on the flow in an impeller and diffuser. J. Turbomach. 109, 48–54.

Speziale, C.G., 1985. Modelling the pressure gradient-velocity correlation of turbulence. Phys. Fluids 28, 69–71.

Speziale, C.G., 1989. Turbulence modelling in noninertial frames of reference. Theoret. Comput. Fluid Dyn. 1, 3–19.

Stepanoff, A.J., 1948. Centrifugal and Axial Flow Pumps: Theory, Design, and Application. Wiley, New York.

Thwaites, B., 1949. Approximate calculation of the laminar boundary layer. Aeronaut. Quart. 1, 245–280.

Visser, F.C., Brouwers, J.J.H., Jonker, J.B., 1999. Fluid flow in a rotating low specific-speed centrifugal impeller passage. Fluid Dyn. Res. 24, 275–292.

Wo, A.M., Bons, J.P., 1993. Flow physics leading to system instability in a centrifugal pump. J. Turbomach. 116, 612–620.

Worster, R.C., 1963. The flow in volutes and its effect on centrifugal pump performance. Proc. Inst. Mech. Engrs 177, 843–865.

Zienkiewicz, O.C., Taylor, R.L., 1989. The Finite Element Method. McGraw-Hill, Maidenhead, UK.